JACS
JOURNAL OF THE AMERICAN CHEMICAL SOCIETY
Article
pubs.acs.org/JACS

Exploring the Formation and Recognition of an Important G-Quadruplex in a HIF1α Promoter and Its Transcriptional Inhibition by a Benzo[c]phenanthridine Derivative

Han Chen,[†] Haitao Long,[†,§] Xiaojie Cui,[†] Jiang Zhou,[†] Ming Xu,[‡] and Gu Yuan*[,†]

[†]Beijing National Laboratory for Molecular Sciences, Key Laboratory of Bioorganic Chemistry and Molecular Engineering of Ministry of Education, Department of Chemical Biology, College of Chemistry and Molecular Engineering, Peking University, Beijing 100871, China

[‡]Key Laboratory of Molecular Cardiovascular Sciences, Ministry of Education, Peking University Third Hospital, 49 North Garden Road, Beijing 100191, China

[§]School of Chemistry, Beijing Institute of Technology, 5 South Zhongguancun Street, Beijing 100081, China

Supporting Information

ABSTRACT: Four putative G-quadruplex sequences (PGSs) in the HIF1α promoter and the 5′UTR were evaluated for their G-quadruplex-forming potential using ESI-MS, CD, FRET, DMS footprinting, and a polymerase stop assay. An important G-quadruplex (S1) has been proven to inhibit HIF1α transcription by blocking AP2 binding. A benzo[c]phenanthridine derivative was found to target the S1 G-quadruplex and induce its conformational conversion from antiparallel to parallel orientation. The transcriptional suppression of HIF1α by this compound was demonstrated using western blotting, Q-RT-PCR, luciferase assay, and ChIP. Our new findings provided a novel strategy for HIF1α regulation and potential insight for cancer therapy.

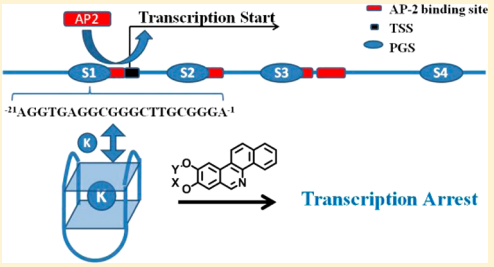

INTRODUCTION

Over the past three decades, HIF1α (hypoxia-inducible factor-1 alpha) has been revealed to be an important target for cancer therapy[1,2] and has attracted exponentially growing interest in the field of cancer biology.[3−5]

HIF1α is the subunit of a heterodimeric protein called HIF1.[6] During normoxia, prolyl hydroxylases (PHDs) hydroxylate the prolyl residues at P402 and P564 of HIF1α and induce degradation via the ubiquitin proteasome pathway.[7] However, during hypoxia, nonhydroxylated HIF1α survives, exhibiting transcriptional activation for more than 70 putative hypoxia-inducible genes, such as VEGF, Glut1, Bcl2, EPO, to affect many cell processes, including angiogenesis, glucose metabolism, antiapoptosis, erythropoiesis, and other functions.[3,8,9] This overexpression behavior has been detected in numerous tumors, including colon, breast, gastric, lung, ovarian, prostate, renal, and pancreatic cancers.[10,11]

In addition to post-transcriptional regulation, the transcriptional activation of HIF1α during hypoxia has also been reported in cell lines including Hep3B, HepG2, HeLa, LN229, and L929.[6,12] The sequence of the HIF1α promoter demonstrates that it belongs to the TATA-less promoter family; this family often depends on Sp1, NF-1, AP2 binding site sequences located up- or downstream from the transcription start site (TSS).[13] The work reported by E. Minet et al. shows that the constitutive transcription of HIF1α is partially mediated by Sp1 binding sites and the other cis-acting elements located within the GC-rich region of the HIF1α promoter and 5′UTR.[14]

Recently, G-quadruplexes (G4) in human genomes were implicated in apoptosis, gene transcription, and gene expression. Many putative G-quadruplex sequences (PGSs) located in the promoters of oncogenes, such as bcl-2, c-myc, c-myb, and c-kit,[15−18] were proven to have potential therapeutic mechanisms and were validated as targeting sites for drugs. A PGS located in the +36 to +56 region (NCBI, gene ID 3091) of HIF1α 5′UTR has been investigated.[19−21] However, the bioinformatics show that there are three other G-rich sequences that contain PGS located in the −20 to −1, +9 to +30, and +481 to 500 regions of HIF1α. In particular, there are two AP2 binding sites that overlap with the −20 to +29 region, enabling their action as a critical cis-acting element for regulating HIF1α expression (Scheme 1).

In this paper, we evaluated the formation of G-quadruplexes from four PGSs in the HIF1α promoter and the 5′UTR, as well as their importance for HIF1α transcription and binding to a transcriptional factor (AP2). In addition, a series of synthetic benzo[c]phenanthridine derivatives were screened as binding candidates for these G-quadruplexes. The inhibition of the transcriptional activity and mechanism on HIF1α were also explored.

Received: November 27, 2013
Published: January 22, 2014

   dx.doi.org/10.1021/ja412128w | J. Am. Chem. Soc. 2014, 136, 2583−2591

Scheme 1. G-Rich Sequences in HIF1α Gene

S1: $^{-21}$AGGTGAGGCGGGCTTGCGGGA^{-1}

S2: $^{+9}$CGGCCTGGGCAGGCGAGCGGGC^{+30}

S3: $^{+57}$CGGGGAGGGGAGAGGGGGCGGGA^{+35}

S4: $^{+501}$AGGGCGGGCAGGCGGGCGGGGT^{+480}

EXPERIMENTAL SECTION

Materials. The MCF-7 cell line, the growth media, and the serum were purchased from Sangon Biotech. The anti-AP2α was purchased from Santa Cruz; anti-HIF1α and anti-β-actin were acquired from Cell Signaling. The oligodeoxygenucleotides (ODNs) were ordered from Sangon Biotech (Supporting Information Table S1). The chemical reagents were purchased from ACROS or Sinopharm Chemical Reagent Beijing Co., Ltd.

Drug Synthesis. The benzo[c]phenanthridine derivatives were synthesized in our laboratory as previously described.[22] The synthetic details were provided in the Supporting Information. The agents used for screening are shown in Chart 1.

Chart 1. Structures of Benzo[c]phenanthridine Derivatives

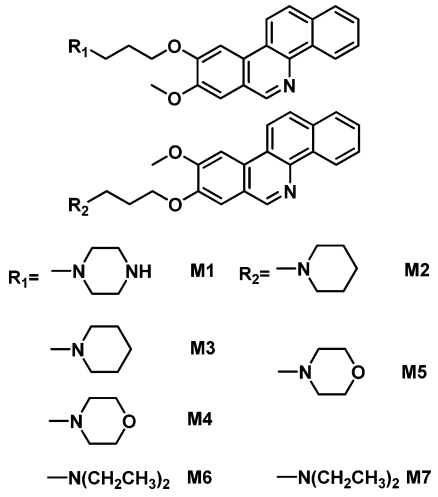

Mass Spectrometry. Normal ESI mass spectra were obtained in negative ion mode with a Finnigan LCQ Deca XP Plus ion trap mass spectrometer (San Jose, CA). The direct infusion flow-rate was 2.0 μL/min. The electrospray source conditions included a 2.7 kV spray voltage and a 120 °C capillary temperature. During all experiments, the scanned mass range was 500−2000 u. The small molecules (**M1**−**M7**) were directly dissolved in methanol to prepare 1 mM stock solution, respectively. The single-stranded ODN was directly dissolved in a mixture containing 25% methanol, 25% ammonium acetate solution (150 mM in final), and 50% ddH_2O. The final concentration of the ODN was 10 μM.

Circular Dichroism. The CD experiments were carried out with a J-815 CD spectrometer (JASCO, Japan); 10 μM ODN (S1−S4, Supporting Information Table S1) was diluted in 150 mM KCl and 30 mM Tris-HCl buffer (pH = 7.4). Afterward, it was annealed at 95 °C for 10 min and slowly cooled to 4 °C over 8 h. To titrate the KCl and small molecules, a series of samples containing 0−150 mM KCl and 0−40 μM **M3** were prepared. The samples were scanned in a 1.0 cm path-length cuvette for three times to obtain the average spectrum from 200 to 400 nm.

FRET. The FRET experiments were carried out using a F7000 fluorescence spectrometer (Hitachi, Japan). A series of samples containing 0−800 mM KCl and 0.5 μM labeled ODN (S1fret, S1fam, S1rox, Supporting Information Table S1) were diluted in 30 mM Tris-HCl buffer (pH = 7.4) and annealed at 95 °C for 5 min before slowly cooling to 4 °C over 8 h. The excitation wavelength for 6-FAM was 485 nm. The samples were scanned at 240 nm/min twice to obtain the average emission spectrum from 500 to 750 nm.

NMR. The NMR experiments were performed on a Bruker AV700 spectrometer (700 MHz) at room temperature. The S1 was dissolved in a solution containing 10% D_2O, 100 mM KCl, and 25 mM potassium phosphate (pH = 7.0) to a final concentration of 1 mM. The 1-D ^{1}H NMR spectrum was collected.

DMS Footprinting. The DMS footprinting assay was performed as previously described.[23,24] The FAM-labeled ODN (S1fam,S1fam2, Supporting Information Table S1) was diluted with 60 mM Tris-HCl buffer (pH = 7.4) to 0.2 μM while containing 0−100 mM salt (LiCl or KCl); afterward, preannealing at 95 °C was performed for 10 min before slowly cooling to 4 °C. The annealed samples were treated with 10% DMS for 5 min before being quenched and extracted with a Tris−phenol−chloroform solution (pH = 8.0). The aqueous phase was precipitated using ethanol at −80 °C. The dry precipitate was dissolved in 10% piperidine and incubated at 90 °C for 30 min, followed by precipitation. The treated sample was resolved using 20% denatured PAGE gel at 1500 V for 4 h in a 4 °C cold room before being imaged with a GE Healthcare Typhoon9400 gel scanner.

Polymerase Stop Assay. A polymerase stop assay was performed as previously described.[25,26] The template (S1t−S4t, Supporting Information Table S1) was diluted with PCR buffer containing 2.5 mM $MgCl_2$, 500 nM PSA primer (Supporting Information Table S1), 0−150 mM KCl, and 0−40 μM small molecules to 200 nM in total volume of 19 μL. The PCR mixture was annealed at 95 °C for 5 min and was slowly cooled to 4 °C over 8 h. Afterward, 1 μL of Taq polymerase was added, and the mixture was incubated at 37 °C for 15 min, followed by quenching on ice. The PCR sample was resolved using 12% denatured PAGE gel at 1500 V for 2 h in a 4 °C cold room before being imaged with a GE Healthcare Tyhoon9400 gel scanner.

Western Blotting. The cultured MCF-7 cell lines were split into six-well plates (~8 × 10^5 cells/well) and incubated at 37 °C overnight. Powdered **M3** was dissolved in ethanol to generate a 10 mM stock solution; this solution was diluted with complete growth medium to form a final working solution (0−20 μM), and ethanol was the control. After the cells settled down, we changed the growth medium in the six-well plate to a drug working solutions from 0 to 20 μM. The cells were maintained in a hypoxia chamber at 37 °C, with 5% CO_2, 1% O_2, and 94% N_2 for 18 h. The samples were using a general harvest procedure with 1× lysis buffer and PMSF. The samples were loaded in a 10% SDS gel and transferred to a nitrocellulose membrane with 1× transfer buffer at 45 V at 4 °C for 18 h. Afterward, the samples were blocked with 5% nonfat milk at room temperature for 1 h and probed with specific primary antibodies at 4 °C overnight. The target proteins were visualized via treatment with an HRP-linked secondary antibody.

Q-RT-PCR. The cultured MCF-7 cells were treated as described above. The total RNA was extracted using Trireagent (Invitrogen) while following the manufacturer's instructions. The concentration of the total RNA was measured with a NanoDrop 1000 (Thermo Scientific). The TransScript II All-in-One First-Strand cDNA Synthesis SuperMix for qPCR (Beijing, Transgen) kits were used for cDNA synthesis in a 20 μL volume with 1 μg total RNA. The mixed samples were incubated at 42 °C for 1 h, heated at 85 °C for 10 min, and stored at −20 °C. Next, 12.5 μL of SYBR Green PCR Master Mix (Applied Biosystem), 10.5 μL H_2O, and 0.5 μL of the forward and reverse primers (Table 1) were mixed and placed in each well of an optical reaction plate. Subsequently, 1 μL of each cDNA sample was added to the well to achieve a final volume of 25 μL. β-Actin was used as a control. The reaction was performed in an Eppendorf Realplex Real-time PCR System.

Luciferase Assay. The luciferase assay was performed as previously described.[27] The pGL4.10-basic vector was purchased from Promega. A 1.6-kb fragment of human HIF1α promoter (from

dx.doi.org/10.1021/ja412128w | J. Am. Chem. Soc. 2014, 136, 2583−2591

Table 1. ESI-MS Screening Results

M1−**M7** targeting to S1 G-quadruplex		**M3** targeting to DNA	
agents	IR_a	DNA	IR_a
M1	0.33	Q1	0.79
M2	0.41	Q2	0.62
M3	0.79	Q3	0.41
M4	0.49	Q4	0.33
M5	0.33	S1 double strand DNA	0.09
M6	0.17		
M7	0.28		

−1041 to +566) was generated via PCR from Hela cells, and four mutation fragments were constructed. The amplified fragments were attached to the Kpn I/Hind III sites of a pGL4.10-basic vector and introduced into *E. coli*. All constructed vectors were verified via automated sequencing.

The cultured MCF-7 cell lines were split into 24-well plates (~1 × 10^4 cells/well) and incubated at 37 °C overnight. To verify the activity of the mutation on the promoter, 400 ng of PGL4.10 or one of the five constructed vectors was transfected into MCF-7 via lipofectamine 2000, and 20 ng of p-RL-TK vector was cotransfected as the internal control. To verify the effect of small molecules on the HIF1α promoter activity, 10 mM of the **M3** stock solution was diluted with complete growth medium to form a final working solution (0−20 μM) that was added to 24-well plates during transfection. The cells were harvested, and the luciferase activity was measured using a Dual-Luciferase Reporter Assay System according to the manufacturer's instructions. The relative activity was normalized using the ratio of Firefly luciferase activity to Renilla luciferase activity and calculated using the folds to control pGL4.10 vector.

Chromatin Immunoprecipitation Assay. The MCF-7 cell line was cultured in 100 mm plates. To verify the effect of small molecular, a 10 mM stock solution of **M3** was diluted with complete growth medium to form a final working solution (0−15 μM). The cells were treated with the working solution and incubated overnight. The general procedure was performed as instruction manual of ChIP Assay kit (#P2078, Beyotime) provided by manufacturer. The treated cells were washed with 9 mL of fresh growth medium containing 4% formaldehyde at room temperature for 10 min, followed by mixing with 1 mL of 10 × glysin buffer and incubation for another 10 min. After removing the growth medium, the cells were resuspended with trypsin and counted. For each sample, 4 × 10^6 cells were lysed via supersonication and diluted with ChIP buffer. The nonspecific protein was precipitated with A+G agarose. The supernatant was mixed with 10 μL of anti-AP2 antibody and rotated overnight in a cold room, followed by antibody collection using 60 μL of A+G agarose. Half of the precipitate was washed sequentially with low salt buffer, high salt buffer, LiCl buffer, and TE buffer before elution with SDS buffer. Afterward, the eluted material was denatured in 5 M NaCl at 65 °C for 4 h and concentrated to 30 μL with a DNA Purification Kit (#D0033, Beyotime). The purified DNA was amplified using PCR with HIF1α promoter primers (Supporting Information Table S1) and resolved on a 6% PAGE gel with a DNA ladder marker of 200−250bp. The remaining precipitate was washed and analyzed via western blotting with an HRP-linked anti-IgG antibody. For the plasmid ChIP assay, the cells were transfected with 2 μg of PGL4.10 or one of the five constructed vectors via lipofectamine 2000 for 6 h, followed by treatment with the drug working solution overnight. The resuspended cells were lysed with SDS buffer, and the nucleic chromatin was removed via centrifugation at 4500 rpm before supersonication.

RESULTS AND DISCUSSION

Formation of G-Quadruplexes in the HIF1α Promoter and 5′UTR Regions. A bioinformatics search of the NCBI database revealed that there are four PGSs (Sx, x = 1−4) in −500 to +500 regions that include the promoter, 5′UTR, and the first exon of HIF1α (Scheme 1). S1 and S2 are very close to the initial transcription site, and S1−3 overlap with the AP2 binding sites; these sites may be critical for regulating the transcription of Hif1α via their secondary structures.[14]

The potential G-quadruplex formation of S1−4 was evaluated by ESI-MS, CD spectrometry, FRET, DMS footprinting, and a polymerase stop assay. In H_2O−CH_3OH (3:1) without NH_4OAc, S1 showed a distinctive pattern including a series of multicharge peaks, revealing an unfolded structure without monovalent cations (Figure 1a). In H_2O−CH_3OH (3:1) with 150 mM NH_4OAc, an ion at m/z =1323 was observed in the mass spectrum, which is the complex ion [S1 + NH_4^+ − $6H^+$]$^{5-}$ (Q1), indicating the formation of a 2-layer G-quadruplex.[28,29] (Figure 1b). In contrast, a mutation of S1, which would completely disrupt the G-quadruplex, only showed a peak at m/z 1320, representing a single S1m without any ammonium ions (Supporting Information Figure S1). The previous work has proven that additional ammonium ions are strong evidence for G-quadruplex formation during ESI-MS analysis.[27−29] The same evidence has been found in S2, S3, and S4, forming 2-, 3-, and 3-layer G-quadruplexes (Q2, Q3, and Q4), respectively (Supporting Information Figure S1).

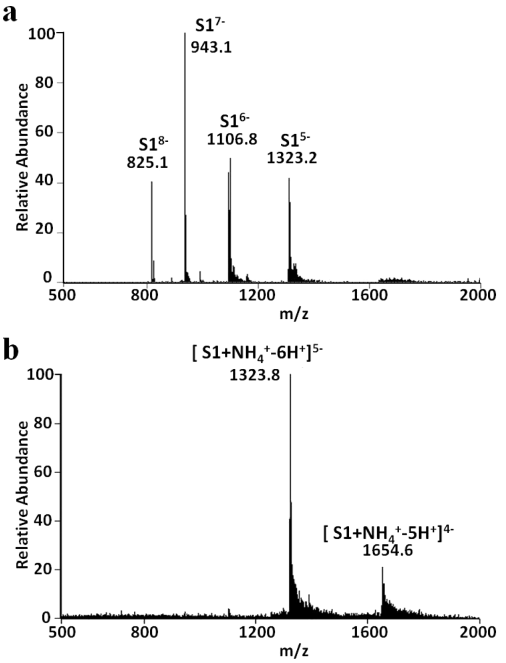

Figure 1. Mass spectra of S1 in H_2O−CH_3OH (3:1) without NH_4OAc (a) and in H_2O−CH_3OH (3:1) with 150 mM NH_4OAc (b).

To confirm the formation of the G-quadruplexes in the HIF1α promoter, CD experiments were performed. The 10 μM solution of S1 in Tris-HCl (30 mM, pH = 7.4) mainly showed a broad positive peak from 240 to 300 nm in the CD spectrum, indicating an unfolded S1 (Figure 2).[30,31] After increasing the concentration of KCl from 0 to 150 mM, the CD spectra of S1 exhibited a dramatic change including an increase at approximately 292 nm and a decrease at approximately 262 nm (Supporting Information Figure S2). In 150 mM KCl, S1 showed positive peaks at 292, 243, and 211 nm and negative peaks at 262 and 230 nm. The strong positive peak at 292 nm revealed that an antiparallel G-quadruplex structure formed in 150 mM KCl (Figure 2).[32] The result of FRET assay confirmed also the formation of S1 G-quadruplex (Supporting Informa-

dx.doi.org/10.1021/ja412128w | J. Am. Chem. Soc. 2014, 136, 2583−2591

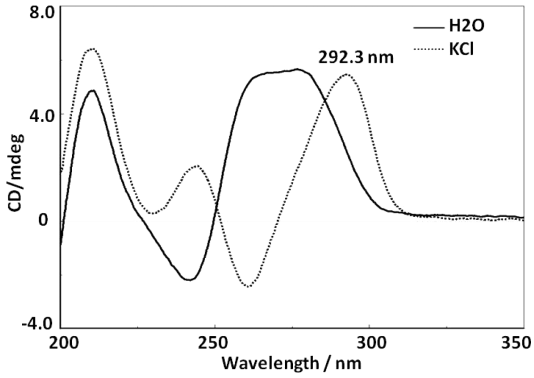

Figure 2. CD spectra of S1 dissolved in 30 mM Tris-HCl buffer (pH = 7.4) to 10 μM. The solid line is the CD spectrum in the absence of KCl, and the dotted line is that in the presence of 150 mM KCl.

tion Figure S3). In addition, S2 showed the formation of an antiparallel G-quadruplex in high concentrations of KCl, while S3 and S4 formed parallel G-quadruplexes with a major peak at 262 nm[30] (Supporting Information Figure S2).

A polymerase stop assay was used to verify the formation of the G-quadruplex. S1, S3, and S4 exhibited strong stop bands with 150 mM KCl, while barely a band was observed without KCl. The blocking of Taq polymerase indicated the formation of a special structure that was induced by KCl, suggesting a stable G-quadruplex (Figure 3a,b).[25] The stop bands for the S3

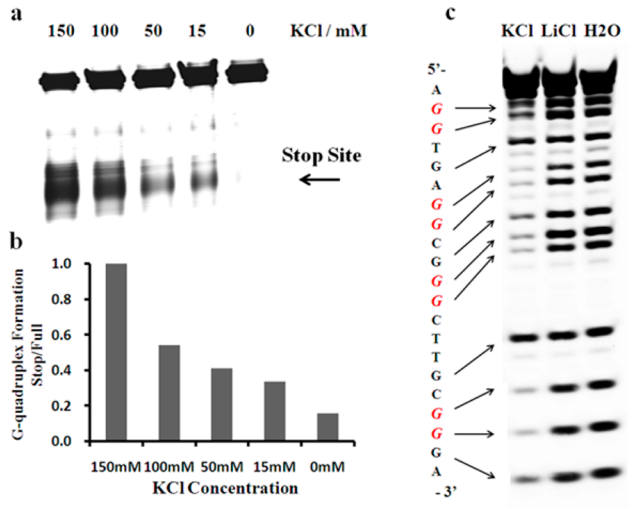

Figure 3. Polymerase stop assay (a) and the relative intensity of the stop bands (b) at various KCl concentrations using S1 template: Extension through the template was arrested as the KCl concentration increased from 0 to 150 mM. The DMS footprinting comparison (c) used 6-FAM labeled S1 incubating in 30 mM Tris-HCl buffer, 150 mM LiCl, or 150 mM KCl to identify the guanosines involved in the G-quadruplex.

and the S4 were clearer than that for the S1, suggesting that the 3-layer G-quadruplex was more stable than the 2-layer G-quadruplex (Supporting Information Figure S4). However, there was no obvious stop band observed for the S2, suggesting an unstable G-quadruplex because of a 2-layer G-quadruplex with long loop.

Because 12 guanosines (5′-AG^{1}G^{2}TG^{3}AG^{4}G^{5}CG^{6}G^{7}G^{8}CTT-G^{9}CG^{10}G^{11}G^{12}A-3′) are present in the S1, and the folding of the guanosines into a G-quarter will produce a smaller surface that is accessible to solvent, protecting these residues from methylation by DMS and diminishing the respective cleaved bands,[24] the DMS footprinting assay was performed to identify which guanosines can be integrated into the G-quadruplex structure. The DMS experiments demonstrated that the S1 sequence forms a G-quadruplex structure in 150 mM KCl, and the 1st, 2nd, 4th, 5th, 7th, 8th, 10th, and 11th guanosines primarily participated in G-quadruplex formation because their bands were weaker than those of the 3rd, 6th, 9th, and 12th guanosines. Both 3′- and 5′-labeled S1 exhibited the same cleavage pattern (Figure 3c and Supporting Information Figure S5). In addition, the NMR spectrum of S1 in KCl solution showed that the peaks of the imino protons at δ 10.8−12.0 ppm corresponded to the eight imino protons of the guanines participating in the S1 G-quadruplex formation, confirming a 2-layer G-quadruplex formed (Supporting Information Figure S6).

G-Quadruplex in the HIF1α Promoter May Regulate the Transcription of HIF1α. Because four PGSs in the HIF1α promoter have been identified and proven to form the 2- or 3-layer G-quadruplex *in vitro*, four mutation plasmids were constructed to investigate their function during the transcription of HIF1α. Each plasmid contained only one mutation in which two GC base pairs were replaced with two TA base pairs on one of the four PGSs, blocking the formation of one of the four G-quadruplexes. Each mutation avoided any possible protein binding sites, as previously reported.[14] The mutation sites are shown in Figure 4a, and the four mutation plasmids were named PS1−PS4.

A dual-luciferase assay was used to evaluate the effect of the mutation on HIF1α transcription. The wild type (WT) and mutation plasmids exhibited 15- to 30-fold fluorescence relative to a blank plasmid (pGL4.10), demonstrating that the inserted fragment maintained the activity of the HIF1α promoter. PS1, PS2, and PS3 showed a higher transcription level than WT, indicating the down-regulation of these PGSs (Figure 4b). However, the PS4 maintained the similar transcription level with that of the WT due to the long distance between this PGS and TSS (approximately 480 bp). Of the up-regulation mutation plasmids, only PS1 was significantly different from the WT ($P < 0.05$), exhibiting an approximate 50% increase in the transcription level relative to the wild type promoter. The mutation at the site of −15 to −14 completely disrupted the G-quadruplex without disrupting the sequence of the HRE (−23 to −17) or AP2 binding site (−10 to −1), reducing the resistance against the transcription inducing by the G-quadruplex while maintaining the activity of the other trans-acting factors. In addition, because the formation of a G-quadruplex may reject protein binding to DNA primary sequence, the absence of the G-quadruplex with keeping binding site may increase the activity of these trans-acting factors, such as AP2. Although PS2 exhibited an increase similar to PS1, the poor P value (approximately 0.11) and the minimal stabilization of the G-quadruplex *in vitro* indicated a very limited effect for this PGS. The PS3 contained multiple G-rich fragments that may form different G-quadruplexes. Although the mutation at +34 to +35 may disrupt the optimal 3-layer G-quadruplex, the 2-layer or long loop G-quadruplex remained a possibility. The increased transcription level induced by PS3 showed that the disruption of the 3-layer G-quadruplex may up-regulate HIF1α, but this trend had been limited by its involute and various structure.

dx.doi.org/10.1021/ja412128w | J. Am. Chem. Soc. 2014, 136, 2583−2591

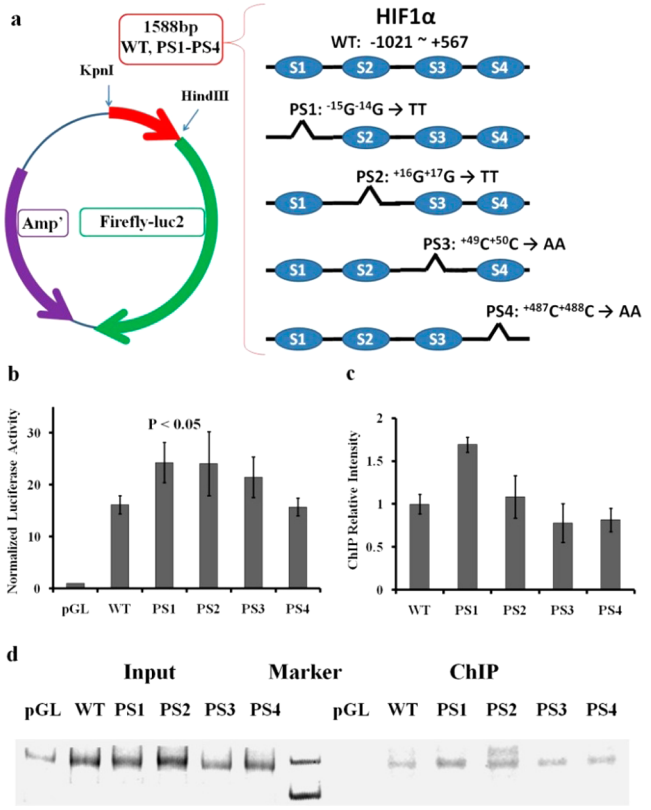

Figure 4. Schematic representation of the constructed luciferase plasmids for WT and PS1−4: (a) each PGS was mutated, and the G-quadruplex was disrupted separately. The relative luciferase activity (b) of the constructed plasmids showed an up-regulated transcription via mutation on S1, S2, and S3. All luciferase assays were conducted in octuplicate and normalized to pGL4.10 control. The plasmid ChIP assay using an anti-AP2 antibody (d) and the PCR product relative intensity (c) showed that mutation of the S1 G-quadruplex enhanced the AP2 binding affinity to HIF1α promoter. All ChIP assays were conducted in triplicate and normalized to WT.

A previous report suggested that AP2 may play a key role during HIF1α transcription,[10,33] and all of the PS1, PS2, or PS3 contain AP2 binding sequence.[12] A plasmid chromatin immunoprecipitation assay was performed to evaluate the binding affinity of AP2 to the wild type and mutation plasmids containing the HIF1α promoter sequence. In the cytoplasm, the plasmids were bound to AP2 and cross-linked with formaldehyde. Subsequently, the AP2 was bound to an anti-AP2 antibody and precipitated via anti-IgG beads. The enriched plasmids were recovered using a high concentration of NaCl at 65 °C followed by purification. The primers for the HIF1α promoter (promoter-f and promoter-r, Supporting Information Table S1) were used for PCR, and the products (230bp) were resolved using PAGE. The higher binding affinity of AP2 for plasmids will generate more enriched plasmids and more intense PCR product bands at 230 bp. Because most of the nucleic DNA was removed before supersonication, and the blank plasmid of pGL4.10 did not contain HIF1α promoter primers binding site, very little PCR product was observed for the blank sample. The AP2 binding affinity was evaluated using the band intensity ratio of the ChIP bands versus the input bands with a blank sample as the background and normalization relative to the WT. Figure 4c,d shows that only PS1 exhibited a notable increase in AP2 affinity, while the other plasmids maintained similar levels, demonstrating that the transcriptional up-regulation of PS1 was primarily mediated by the AP2 pathway; the −10 to −1 region was a key cis-element that was regulated by the competition between the G-quadruplex and the AP2.

Recognition of the HIF1α G-Quadruplex by Benzo[*c*]-phenanthridine Derivatives. A series of benzo[*c*]-phenanthridine derivatives were used to select the recognition molecules that bind to the HIF1α G-quadruplexes. Each of these small molecules was mixed with the HIF1α G-quadruplex and analyzed using ESI-MS. Figure 5a and Supporting

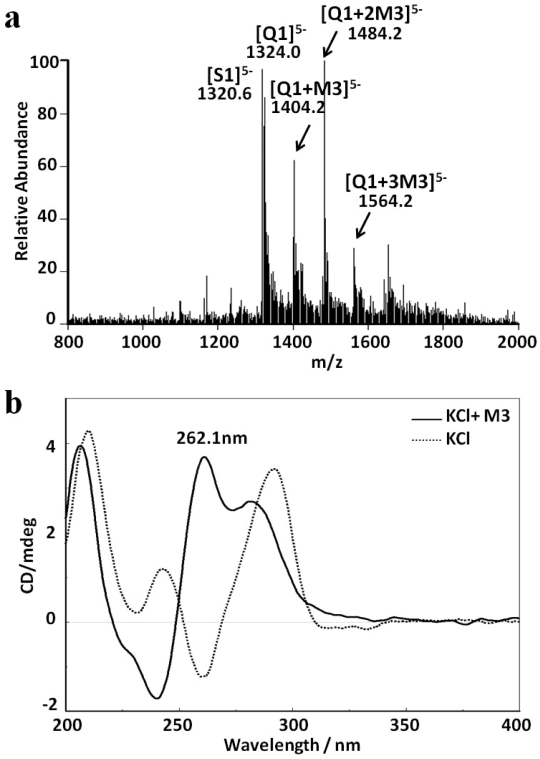

Figure 5. (a) ESI mass spectrum of **M3** bound to the S1 G-quadruplex: the S1 was dissolved in H_2O−CH_3OH (3:1) with 150 mM NH_4OAc, and the ligand−S1 ratio was 2:1. (b) The CD spectrum of 5 μM S1 mixed with (solid line) or without (dotted line) 40 μM **M3** in 30 mM Tris-HCl and 50 mM KCl buffer showed that **M3** could induce the conformational change of the S1 G-quadruplex from antiparallel to parallel orientation.

Information Figure S7 showed parts of the ESI mass spectra for the mixtures containing the S1 and the small molecules in a 1:2 molar ratio as examples. The relative intensity of the complex ion of Q1 with **M3** is 100% in the mass spectrum, indicating that **M3** has a high affinity for the S1 G-quadruplex. Its primary binding mode is 1:2, as characterized by a base peak at m/z 1484 that represents a complex ion ($[S1 + NH_4^+ + 2\mathbf{M3} - 6H^+]^{5-}$). The 1:1 and 1:3 species were also observed at m/z 1404 and 1564, representing $[S1 + NH_4^+ + \mathbf{M3} - 6H^+]^{5-}$ and $[S1 + NH_4^+ + 3\mathbf{M3} - 6H^+]^{5-}$, respectively. **M1** and **M2** also showed a series peaks of the complex ions with Q1 at the 40−50% relative intensity; however, the relative intensity of the complex ions for **M6** with Q1 was much weaker, indicating poor affinity.

To evaluate the binding affinity of small molecules (**M***x*, x = 1−7) to the G-quadruplex (Qx, x = 1−4), IR_a was defined as

dx.doi.org/10.1021/ja412128w | J. Am. Chem. Soc. 2014, 136, 2583−2591

the relative abundance ratio of all the bound ions (n = 1−3) to that of both unbound and bound species (n = 1−3).[27]

$$IR_a = \frac{I_r[Qx + n\mathbf{M}x]^{5-}}{I_r[Sx]^{5-} + I_r[Qx]^{5-} + \sum I_r[Qx + n\mathbf{M}x]^{5-}}$$

The $I_r[Qx + n\mathbf{M}x]^{5-}$ was the integral intensity of the complex ion of Qx−$\mathbf{M}x$ at molar ratio of 1:n in the ESI mass spectrum. The $I_r[Sx]^{5-}$ and the $I_r[Qx]^{5-}$ were the integral intensity of Sx and Qx (x = 1−4). The maximum value of IR_a is 1.00, the nearer the IR_a value to 1.00, the higher the binding affinity of $\mathbf{M}x$ to Qx.

The IR_a values of the benzo[c]phenanthridine derivatives binding to Q1 were shown in Table 1. In these derivatives, only **M3** was a preferable candidate for binding Q1 with a highest IR_a at 0.79, while those of the other derivatives were lower than 0.5.

The binding selectivity for **M3** to the S1−4 G-quadruplexes (Q1−4) and the double strand of S1 were also evaluated by ESI-MS. Table 1 summarized the IR_a values for **M3** binding with Q1−4 and the S1 double-stranded DNA, which revealed that **M3** had the best binding affinity (IR_a = 0.79) with the S1 G-quadruplex (Q1), while Q2 showed the lower IR_a of 0.62. The binding affinities of **M3** to Q3 and Q4 were much weaker than that of Q1. The S1 double stranded bound to **M3** was barely observed (IR_a = 0.09). These results illustrated that **M3** had a selective and high binding affinity for the S1 G-quadruplex. It could bind primarily to the S1 G-quadruplex in the HIF1α promoter.

In addition to the binding affinity and selectivity, the small molecule-induced structural changes of the S1 G-quadruplex were investigated using CD spectra. The S1 can form antiparallel G-quadruplex in KCl. However, when **M3** was added to the S1 G-quadruplex, this small molecule could induce the structural change of the G-quadruplex. Supporting Information Figure S8c shows the titration of 0 to 40 μM **M3** in 5 μM the G-quadruplex. While increasing the concentration of **M3**, the positive peak for the G-quadruplex at 292 nm was weakened and moved to a shorter wavelength, while the negative peak at approximately 260 nm was changed to a positive peak to become the major peak. With 40 μM **M3**, the G-quadruplex showed a strong positive peak at 262 nm, a shoulder peak at 279 nm, and a negative peak at 240 nm, indicating the orientation of the strands had been changed from antiparallel to parallel (Figure 5b).[30] KCl was needed for the conversion because **M3** cannot induce a G-quadruplex without any positive ions to drive G-quadruplex formation. However, high concentrations of KCl hindered the conversion because potassium may induce an antiparallel structure and offset the effect of **M3**. With the complementary strand of S1, the CD spectrum showed a broad peak at 280 nm, indicating the formation of double stranded DNA from S1 and S1c (Supporting Information Figure S8a). Adding **M3** to this solution generates a shoulder peak at approximately 260 nm, demonstrating that **M3** can partially induce G-quadruplex formation in the S1 double strand. The induced S1 conformational change was a unique property of **M3**; the other benzo[c]phenanthridine derivatives barely affected the antiparallel G-quadruplex of the S1. The structural shift may be important to its function during HIF1α transcription.

A DMS footprinting assay was used to identify the **M3** binding site on the S1 G-quadruplex. The annealed S1fam was incubated with 50 mM KCl and 40 μM **M3** overnight before treatment according to the general procedure for DMS footprinting. Except for G2 and G9, all guanosine cleavage bands faded in the presence of **M3** due to the multibinding mode of **M3** demonstrated by ESI-MS. In particular, G4−G8 almost completely disappeared, suggesting that the 5′-GGCGGG-3′ fragment was the primary binding site for **M3**. However, G9 showed an enhanced cleavage signal due to its location on a large side loop, which swings outward from the G-quadruplex (Figure 6 and Supporting Information Figure S9).

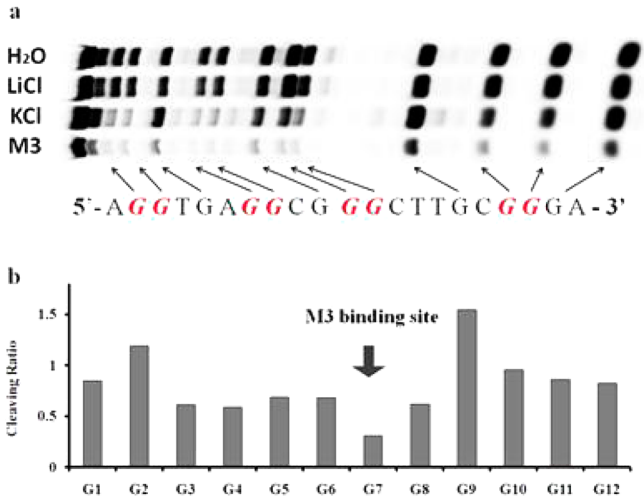

Figure 6. DMS footprinting of S1fam2 in H_2O, 50 mM LiCl, 50 mM KCl, or 50 mM KCl with 40 μM **M3** (a) and the relative cleaving band intensity of the sample in KCl with **M3** normalized to that in KCl without **M3** (b) showed a decrease in cleavage around G4−G8, revealing the binding site of **M3**.

Biological Activity of the Benzo[c]phenanthridine Derivatives on the HIF1α Pathway. To determine whether the benzo[c]phenanthridine derivatives suppress the expression of HIF1α in human cancer cells, a Q-RT-PCR screen was performed using **M1** through **M7** at 15 μM. **M3** showed the best suppression with an approximate 50% decrease in HIF1α transcription, agreeing with the ESI-MS data shown above (Figure 7a).

To confirm whether **M3** can inhibit the expression of HIF1α, both western blots and Q-RT-PCR were applied using human MCF-7 cell line. **M3** significantly inhibited the expression of HIF1α during hypoxia for both mRNA and protein levels (Figure 7b,c). The IC_{50} of the **M3** inhibition of HIF1α was approximately 15 μM, as determined by western blot and Q-RT-PCR. Compound **M3** also inhibited the transcription of VEGF and GluT1 but barely affected the expression of AP2, indicating that **M3** selectively inhibited the expression of HIF1α and blocked the transcription of its downstream genes, such as VEGF, without suppressing its upstream regulators, such as AP2 (Figure 7).

A luciferase assay was used to determine whether **M3** could regulate HIF1α transcription in with or without the S1 G-quadruplex. The WT and PS1 plasmids were transfected into MCF-7 in parallel, and the transcription level was measured. After increasing the concentration of **M3** from 0 to 15 μM, the WT transcription was almost completely inhibited, while PS1 kept more than 50% of its activity (Figure 8a). After normalization with the untreated group, the cells transfected with the S1 mutation plasmid exhibited approximately 8-fold

dx.doi.org/10.1021/ja412128w | J. Am. Chem. Soc. 2014, 136, 2583−2591

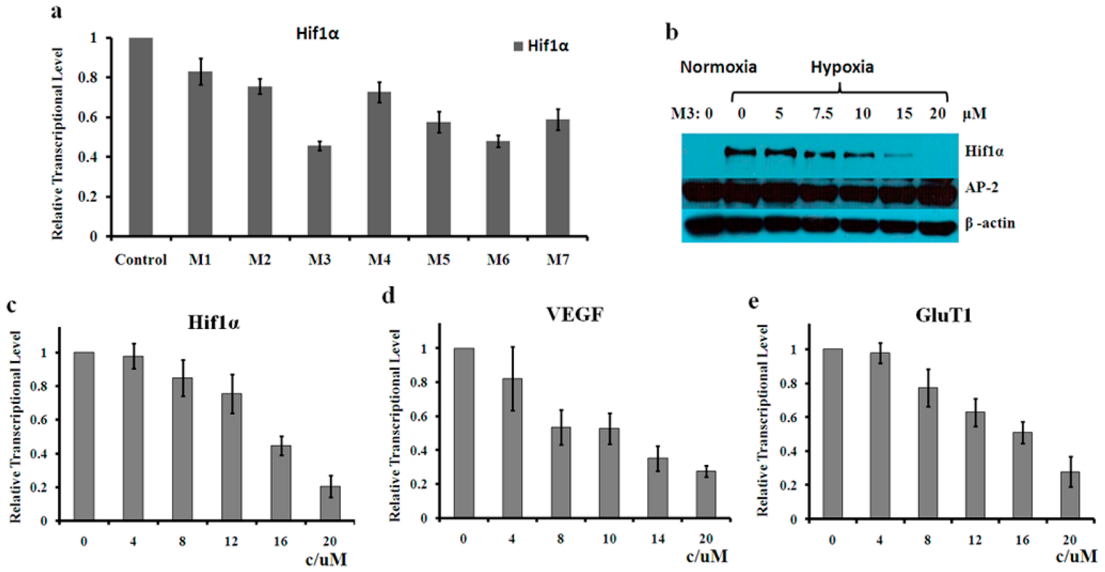

Figure 7. Ligand screening by Q-RT-PCR (a) showed that **M3** can suppress the transcription of HIF1α. The dose-dependent Q-RT-PCR assay (b) and western blot (c) showed that **M3** inhibited HIF1α on mRNA and the protein level along when increasing the **M3** concentration from 0 to 20 μM, while decreasing the transcription of the genes downstream from HIF1α, such as VEGF (d) and GluT1 (e), without affecting the upstream AP2 protein (b). β-Actin was used as control. All Q-RT-PCR assays were conducted in triplicate on the MCF-7 cell line and normalized to an ethanol control. Error bars represent standard deviations.

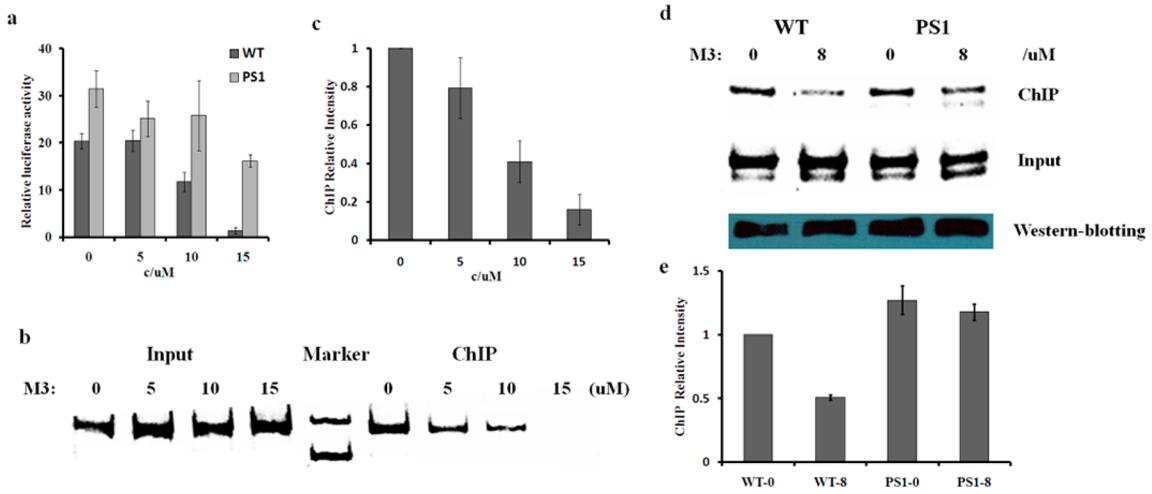

Figure 8. A luciferase assay (a) showed the mutation plasmid PS1 exhibited a stronger transcriptional activity than WT as the concentration of **M3** increased from 0 to 15 μM in the MCF-7 cell line, indicating that **M3** targeted the S1 G-quadruplex and suppressed the transcription of HIF1α. A ChIP assay using an anti-AP2 antibody (b) and the PCR product relative intensity (c) demonstrated that **M3** prevented AP2 from binding to the HIF1α promoter when increasing its concentration **M3** from 0 to 15 μM. The plasmid ChIP assay using an anti-AP2 antibody with a WT and a PS1 plasmid (d) showed that the AP2 binding affinity was maintained in the S1 mutation plasmid (PS1) compared to WT after treatment with 8 μM **M3** (e), indicating that **M3** can bind to the S1 G-quadruplex and block AP2. WT-0, WT-8, PS1−0, and PS1−8 stand for the MCF-7 cells treated with WT, WT followed by 8 μM **M3**, PS1, and PS1 followed by 8 μM **M3**, respectively.

resistance compared to the WT against 15 μM **M3**, demonstrating that the S1 G-quadruplex might be a primary target for **M3** during cellular HIF1α transcription and confirming the biological activity of **M3**. However, both the WT and PS1 showed a significant decrease in transcription when the concentration of the **M3** exceeded 15 μM, possibly due to the weak binding affinity of **M3** for other PGSs in the HIF1α promoter.

To determine the mechanism of inhibition for **M3** on HIF1α transcription, a ChIP assay was performed using an MCF-7 cell line. After being normalized by the input PCR products, the concentration of the ChIP PCR products decreased dramatically as the concentration of **M3** increased (Figure 8b,c). The IC_{50} measured by a ChIP assay was approximately 7.5 μM, remaining lower than the IC_{50} value identified via western blotting and Q-RT-PCR. Therefore, **M3** is an efficient transcriptional inhibitor for HIF1α because it blocks the AP2 pathway.

Plasmid ChIP was also used to evaluate the inhibition of **M3** on the transcription of the S1 mutation plasmid. The WT and PS1 plasmid binding with AP2 was assessed: the PCR products were amplified and were quantified using the AP2 abundance determined by western blotting. Because **M3** binds and converts the conformation of the S1 G-quadruplex but not

dx.doi.org/10.1021/ja412128w | J. Am. Chem. Soc. 2014, 136, 2583−2591

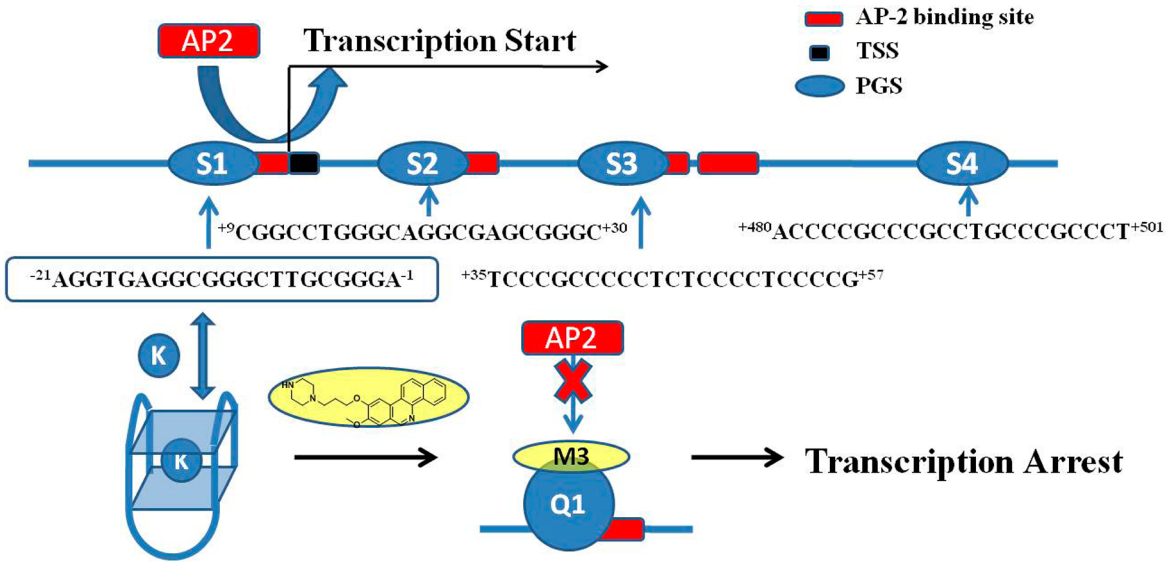

Figure 9. Mechanism of HIF1α transcriptional inhibition by the S1 G-quadruplex (Q1) and benzo[*c*]phenanthridine derivative (**M3**): The S1 PGS is overlapped with an AP2 binding site, and the formation of the S1 G-quadruplex (Q1) induced by potassium or benzo[*c*]phenanthridine derivative (**M3**) will prevent AP2 from binding to the HIF1α promoter.

the S1 double strand, its binding affinity to the mutated plasmid should be greatly decreased, promoting AP2 binding to the HIF1α promoter. As shown in Figure 8d, after treatment with 8 μM **M3**, the AP2 binding to the WT decreased to 50%, while the AP2 binding to PS1 retained more than 90%, demonstrating that **M3** can bind to the S1 G-quadruplex, prevent AP2 from binding to this cis-element, and suppress HIF1α transcription (Figure 9).

CONCLUSION

We have evaluated the properties of four PGSs in the HIF1α promoter and 5′UTR using multiple spectroscopic and biochemical methods, demonstrating the formation of the antiparallel G-quadruplexes with S1 and S2, as well as parallel G-quadruplexes with S3 and S4. We have proven that the S1 is an important PGS for HIF1α transcription via the formation of a G-quadruplex and blocking the AP2 binding site with both a luciferase assay and a plasmid ChIP analysis. In addition, a benzo[*c*]phenanthridine derivative (**M3**) was screened out, which can bind to the S1 G-quadruplex and induce its structural change, forming a mixed parallel/antiparallel conformation. This compound can primarily inhibit HIF1α transcription by disrupting the AP2 binding site on the G-quadruplex in the S1 sequence. This study provided an important foundation for understanding the biological roles of the HIF1α G-quadruplex, generating potential insight for cancer therapy.

ASSOCIATED CONTENT

Supporting Information

Table of the ODN list, additional figures, synthesis of **M1**−**M7**, and MS and NMR data of **M1**−**M7**. This material is available free of charge via the Internet at http://pubs.acs.org.

AUTHOR INFORMATION

Corresponding Author

guyuan@pku.edu.cn

Notes

The authors declare no competing financial interest.

ACKNOWLEDGMENTS

This work was supported by the 973 Program (2012CB720600, 2012CB720601) and the National Natural Science Foundation of China (21372021).

REFERENCES

(1) Melillo, G. *Methods Enzymol.* **2007**, *435*, 385.
(2) Onnis, B.; Rapisarda, A.; Melillo, G. *J. Cell Mol. Med.* **2009**, *13*, 2780.
(3) Semenza, G. L. *Nat. Rev. Cancer* **2003**, *3*, 721.
(4) Semenza, G. L.; Wang, G. L. *Mol. Cell. Biol.* **1992**, *12*, 5447.
(5) Harris, A. L. *Nat. Rev. Cancer* **2001**, *2*, 38.
(6) Wang, G. L.; Jiang, B. H.; Rue, E. A.; Semenza, G. L. *Proc. Natl. Acad. Sci. U.S.A.* **1995**, *92*, 5510.
(7) Semenza, G. L. *Curr. Opin. Cell Biol.* **2001**, *13*, 167.
(8) Hirotaa, K.; Semenza, G. L. *Crit. Rev. Oncol. Hematol* **2005**, *59*, 15.
(9) Chen, C.; Alireza, N. P.; Behrooz; Ismail-Beigi, F.; Maity, A. *J. Biol. Chem* **2001**, *276*, 9519.
(10) Gruber, M.; Simon, M. C. *Curr. Opin. Hematol.* **2006**, *13*, 169.
(11) Hirota, K.; Semenza, G. L. *Crit. Rev. Oncol. Hematol.* **2006**, *59*, 15.
(12) Wenger, R. H.; Kvietikova, I.; Roles, A.; Gassmann, M.; Marti, H. H. *Kidney Int.* **1997**, *51*, 560.
(13) Iyer, N. V.; Leung, S. W.; Semenza, G. L. *Genomics* **1998**, *52*, 159.
(14) Minet, E.; Michel, G.; Roland, I.; Remacle, J.; Raes, M.; Michiels, C. *Biochem. Biophys. Res. Commun.* **1999**, *261*, 534.
(15) Dai, J.; Jones, R. A.; Hurley, L. H.; Yang, D. Z. *Nucleic Acids Res.* **2006**, *34*, 5133.
(16) Dexheimer, T. S.; Hurley, L. H. *J. Am. Chem. Soc.* **2006**, *128*, 5404.
(17) Fernando, H.; Reszka, A. P.; Huppert, J.; Ladame, S.; Rankin, S.; Venkitaraman, A. R.; Neidle, S.; Balasubramanian, S. *Biochemistry* **2006**, *45*, 7854.
(18) Phan, A. T.; Burge, S.; Neidle, S.; Patel, D. J. *J. Am. Chem. Soc.* **2007**, *129*, 4386.
(19) Armond, R. D.; Sun, D.; Hurley, L. H.; Ebbinghaus, S. W. *Biochemistry* **2005**, *44*, 16341.
(20) Welsh, S. J.; Lombardo, C. M.; Valentine, H.; Fuente, M.; Schatzlein, A.; Neidle, S. *Sci. Rep* **2013**, *3*, 2799.

(21) Lombardo, C. M.; Welsh, S. J.; Strauss, S. J.; Dale, A. G.; Todd, A. K.; Nanjunda, R.; Wilson, W. D.; Neidle, S. *Bioorg. Med. Chem. Lett.* **2012**, *22*, 5984.
(22) Nakanishi, T.; Suzuki, M. *Org. Lett.* **1999**, *1*, 985.
(23) Wang, F.; Zeng, Z.; Wu, R.; Xue, Y.; Hao, Y.; Pang, D.; Zhao, Y.; Tan, Z. *Proc. Natl. Acad. Sci. U.S.A.* **2012**, *109*, 20413.
(24) Kim, M. Y.; Gleason-Guzman, M.; Izbicka, E.; Nishioka, D.; Hurley, L. H. *Cancer Res.* **2003**, *63*, 3247.
(25) Han, H.; Hurley, L. H.; Salazar, M. *Nucleic Acids Res.* **1999**, *27*, 537.
(26) Weitzmann, M. N.; Woodford, K. J.; Usdin, K. *J. Biol. Chem.* **1996**, *271*, 20958.
(27) Lin, S.; Gu, H.; Xu, M.; Cui, X.; Zhang, Y.; Gao, W.; Yuan, G. *PLoS One* **2012**, *7*, e31201.
(28) Rosu, F.; Gabelica, V.; Houssier, C.; Colson, P.; De Pauw, E. *Rapid Commun. Mass Spectrom.* **2002**, *16*, 1729.
(29) Gabelica, V.; Maeda, R.; Fujimoto, T.; Yaku, H.; Murashima, T.; Sugimoto, N.; Miyoshi, D. *Biochemistry* **2013**, *52*, 5620.
(30) Paramasivan, S.; Rujan, I.; Bolton, P. H. *Methods* **2007**, *43*, 324.
(31) Busson, P.; Wu, J.; Wang, C.; Li, X.; Song, Y.; Wang, W.; Li, C.; Hu, J.; Zhu, Z.; Li, J.; Zhang, W.; Lu, Z.; Yang, C. J. *PLoS One* **2012**, *7*, 46393.
(32) Vorlickova, M.; Kejnovska, I.; Sagi, J.; Renciuk, D.; Bednarova, K.; Motlova, J.; Kypr, J. *Methods* **2012**, *57*, 64.
(33) Sperling, S.; Grimm, C. H.; Dunkel, I.; Mebus, S.; Sperling, H. P.; Ebner, A.; Galli, R.; Lehrach, H.; Fusch, C.; Berger, F.; Hammer, S. *Hum. Mutat.* **2005**, *26*, 575.